AMERICAN SOCIETY FOR MICROBIOLOGY | mBio®

RESEARCH ARTICLE

Metabolic Model of the Nitrogen-Fixing Obligate Aerobe *Azotobacter vinelandii* Predicts Its Adaptation to Oxygen Concentration and Metal Availability

Alexander B. Alleman,[a] Florence Mus,[a] John W. Peters[a]

[a]Institute of Biological Chemistry, Washington State University, Pullman, Washington, USA

ABSTRACT There is considerable interest in promoting biological nitrogen fixation (BNF) as a mechanism to reduce the inputs of nitrogenous fertilizers in agriculture, but considerable fundamental knowledge gaps still need to be addressed. BNF is catalyzed by nitrogenase, which requires a large input of energy in the form of ATP and low potential electrons. Diazotrophs that respire aerobically have an advantage in meeting the ATP demands of BNF but face challenges in protecting nitrogenase from inactivation by oxygen. Here, we constructed a genome-scale metabolic model of the nitrogen-fixing bacterium *Azotobacter vinelandii*, which uses a complex respiratory protection mechanism to consume oxygen at a high rate to keep intracellular conditions microaerobic. Our model accurately predicts growth rate under high oxygen and substrate concentrations, consistent with a large electron flux directed to the respiratory protection mechanism. While a partially decoupled electron transport chain compensates for some of the energy imbalance under high-oxygen conditions, it does not account for all substrate intake, leading to increased maintenance rates. Interestingly, the respiratory protection mechanism is required for accurate predictions even when ammonia is supplemented during growth, suggesting that the respiratory protection mechanism might be a core principle of metabolism and not just used for nitrogenase protection. We have also shown that rearrangement of flux through the electron transport system allows *A. vinelandii* to adapt to different oxygen concentrations, metal availability, and genetic disruption, which cause an ammonia excretion phenotype. Accurately determining the energy balance in an aerobic nitrogen-fixing metabolic model is required for future engineering approaches.

IMPORTANCE The world's dependence on industrially produced nitrogenous fertilizers has created a dichotomy of issues. First, parts of the globe lack access to fertilizers, leading to poor crop yields that significantly limit nutrition while contributing to disease and starvation. In contrast, abundant nitrogenous fertilizers and associated overuse in large agricultural systems result in compromised soil quality and downstream environmental issues. Thus, there is considerable interest in expanding the impacts of BNF to promote improved crop yields in places struggling with access to industrial fertilizers while reducing fertilizer input in areas where overuse results in the degradation of soil health. A more robust and fundamental understanding of BNF biochemistry and microbial physiology will enable strategies to promote new and more robust associations between nitrogen-fixing microorganisms and crop plants.

KEYWORDS aerobes, ammonia excretion, bioenergetics, diazotrophs, metabolic modeling, nitrogen fixation, respiration

In agriculture, nitrogenous fertilizers have become essential to maximizing crop yields to support the growing world population (1). Biological nitrogen fixation (BNF) is the reduction of atmospheric dinitrogen (N_2) to ammonia (NH_3) and accounts for ~60% of

Editor Jianping Xu, McMaster University

Address correspondence to John W. Peters, jw.peters@wsu.edu.

The authors declare no conflict of interest.

This article is a direct contribution from John W. Peters, a Fellow of the American Academy of Microbiology, who arranged for and secured reviews by Michael McInerney, University of Oklahoma, and Robert Hausinger, Michigan State University.

Received 12 October 2021
Accepted 3 November 2021
Published 14 December 2021

the fixed nitrogen input into natural ecosystems (2). Nitrogenase, the enzyme catalyzing N_2 reduction, is a significant energy sink, as it requires large amounts of ATP and low-potential electrons to produce NH_3.

There are three types of nitrogenase, termed Mo-, V-, and Fe-only nitrogenases, reflecting the metal cofactor composition in the N_2 reduction catalyst (3–5). Bacteria that contain V- and Fe-only nitrogenases are not dependent on Mo availability in the environment (6). Despite the similar features shared by the three nitrogenases, they differ in their reaction stoichiometry (7, 8). Whereas Mo-nitrogenase is the most efficient, requiring a minimum of 8 low-potential electrons and 16 MgATP to convert N_2 to 2 NH_3 *in vitro* (equation 1), the V- and Fe-only nitrogenases have lower catalytic activities and different reaction stoichiometries, requiring more electrons and ATP for catalysis and producing more H_2 relative to NH_3.

$$N_2 + 8e^- + 16\mathrm{MgATP} + 8H^+ \rightarrow 2NH_3 + H_2 + 16\mathrm{MgADP} + 16P_i \quad (1)$$

Diazotrophs are physiologically diverse and include obligate aerobes, facultative anaerobes, anaerobic heterotrophs, anoxygenic or oxygenic phototrophs, and chemolithotrophs (9, 10). Under nitrogen-fixing conditions, diazotrophs must remodel their energy metabolism to provide nitrogenase with ATP and low-potential electrons while protecting the enzyme from irreversible inactivation by oxygen (11). Oxygen protection is not an issue for strict anaerobes; however, the ATP demands of nitrogen fixation during anaerobic metabolisms, such as fermentation, are profound relative to the ATP production per unit carbon (9). In contrast, oxygen respiration and the light reactions of photosynthesis can generate more energy for diazotrophic growth, but protecting nitrogenase from oxygen inactivation then becomes a larger consideration. Diazotrophs that live in the air protect nitrogenase from inactivation through various mechanisms that involve conditionally, temporally, or spatially separating oxidative phosphorylation or photosynthesis from nitrogen fixation (12).

The ubiquitous soil bacterium *Azotobacter vinelandii* is arguably one of the most robust and productive free-living nitrogen-fixing organisms (13, 14). *A. vinelandii* possesses a greater capacity to fix nitrogen than many other diazotrophs because of its ability to fix nitrogen at high oxygen concentrations (15). This ability is dependent on multiple mechanisms to protect nitrogenase from inactivation by oxygen (11, 16–18, 67). One of the primary mechanisms involves harnessing a robust and dynamic respiratory metabolism to balance the increased energy demands of nitrogen fixation while simultaneously consuming a significant amount of oxygen at the membrane. This process, termed respiratory protection, maintains high enough respiration rates to sustain low oxygen tensions in the cytoplasm (11). A branch of the electron transport chain increases oxygen consumption by partially decoupling ATP synthesis from O_2 consumption (14, 19). To supply energy for respiratory protection, *A. vinelandii* catabolizes sugars through the Entner-Doudoroff and pentose phosphate pathways to produce acetyl coenzyme A (acetyl-CoA) and then predominately uses the tricarboxylic acid (TCA) cycle to deliver NADH (20, 21). During diazotrophic growth, *A. vinelandii* must efficiently balance the reduction of low-potential electron carriers, ATP production using oxidative phosphorylation, and protecting the nitrogenase enzyme from oxygen through the partially coupled branch of the electron transport chain.

A. vinelandii adjusts respiration through a branched respiratory chain that includes multiple dehydrogenases and terminal oxidases. The chain's two branches are classified as (i) the fully coupled branch and (ii) the partially coupled branch, respective to the protons translocated during oxidative phosphorylation (16) (Fig. 1). The branches of the respiratory chain are mediated by two distinct NADH:quinone redox reaction complexes (NDH). The first, NDHI, is coupled to the transmembrane proton potential and is mechanistically similar to complex I of mitochondria (22). However, the second, NDHII, is induced under high-aeration conditions and carries out NADH oxidation without translocating protons across the membrane, thus decoupling oxygen consumption from ATP generation (19). Other dehydrogenases (DHs) can also donate to the quinone pool,

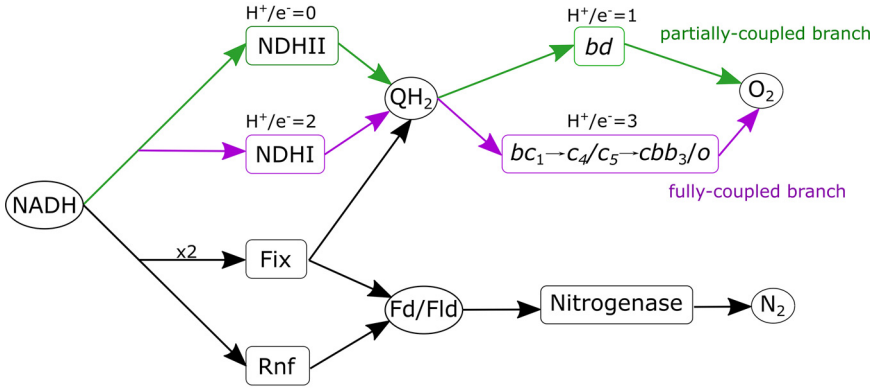

FIG 1 Paths of electrons in the electron transport system of *A. vinelandii*. Four different enzymes potentially consume NADH: uncoupled type II NADH dehydrogenase (NDHII), fully coupled NADH dehydrogenase (NDHI), flavin-based electron bifurcating Fix enzyme complex (Fix), and NADH: ferredoxin oxidoreductase (Rnf). There are two branches of the electron transport system (ETS) that perform oxygen reduction: (i) the partially coupled respiratory protection branch (green), beginning with NDHII reducing quinone to quinol (QH_2) and terminating with cytochrome *bd*, and (ii) the fully coupled branch (purple), beginning with NDHI reducing quinone, in turn reducing cytochrome *c* and ending in cytochrome *o*-like terminal oxidase. Each branch translocates a different number of protons per electron, given above the reaction names. Production of reduced Fd/Fld occurs through enzyme complexes Fix and Rnf, which use NADH as the electron source. Nitrogenase consumes eight reduced Fd/Fld to reduce N_2 to NH_4^+.

including malate DH, succinate DH, and hydrogenases. However, the first two of these DHs do not increase in expression under nitrogen-fixing conditions. However, H_2 production is an obligatory part of the nitrogenase reaction (equation 1), and uptake hydrogenases recycle electrons from the H_2 produced back into the quinone pool (23, 24).

The respiratory chain in *A. vinelandii* branches into two paths from the quinone pool, the fully coupled branch, including the bc_1 complex, cytochrome c_4/c_5, and *o*-type or cbb_3 terminal oxidases, and the partially coupled branch, with cytochrome *bd* (a quinol terminal oxidase). Cytochrome *bd* accumulates under high-aeration conditions, and knockout mutants lacking *bd* oxidase cannot grow diazotrophically at any aeration rate (13, 14, 25). The fully coupled respiratory branch terminates in a classical cytochrome bc_1 reduction of cytochrome *c* to a terminal oxidase of cytochrome *o* or cbb_3 (26). This branch has not been as well characterized in *A. vinelandii*. Still, kinetic evidence *in vivo* supports the existence of two cytochrome *c* terminal oxidases (13). Overall, the fully coupled branch consists of NDHI, cytochrome bc_1, and cytochrome *o*/cbb_3 translocating 10 H^+ per $^1/_2O_2$ reduced, while the partially coupled branch consists of NDHII and cytochrome *bd* and only translocates $2H^+$ per $^1/_2O_2$ reduced (Fig. 1).

Under nitrogen-fixing conditions, *A. vinelandii* carbon catabolism directs most electrons to the reduction of NAD^+, which has a reduction midpoint potential of ~-320 mV, while nitrogenase requires electrons with a lower potential of ~-500 mV (27). Thus, additional energy is required to transfer electrons from NADH to lower potential electron carriers, such as ferredoxin (Fd) or flavodoxin (Fld). Under nitrogen-fixing conditions, *A. vinelandii* expresses membrane-associated Fix and Rnf complexes that catalyze the endergonic reduction of Fd/Fld by NADH (28, 29). Rnf uses the proton motive force to provide the additional energy required in the reaction (30–32). The Fix complex uses flavin-based electron bifurcation in which it catalyzes the coordinated transfer of electrons from NADH to both quinone and Fd/Fld (29). The combination of branched electron transport to oxygen and the generation of reduced Fd/Fld through Fix and Rnf creates a complex and dynamic electron transport system (ETS) (Fig. 1).

The metabolic energy cost of nitrogen fixation in *A. vinelandii* was recently studied through carbon-based metabolomics (20) and investigated through multiple quantitative and metabolic models (33–35). However, these studies did not account for the dynamics of *A. vinelandii*'s ETS and its energy requirements; thus, they lack insights into

TABLE 1 Growth rates and physiological parameters are predicted from flux balance analysis results[a]

	Growth rate (h^{-1})	
Model	**Ammonia supplemented**	**Diazotrophic**
Exptl[b]	0.27	0.25
iDT1278	1.87	1.28
iAA1300		
No added constraints	1.43	0.98
ED and GS constrained	1.37	0.93
ED, GS, and maintenance constrained[c]	0.38	0.24

[a]All models have a glucose uptake rate of 15 $mmol_{glucose} \cdot h^{-1} \cdot g\ CDW^{-1}$. ED, Entner-Doudoroff; GS, glyoxylate shunt.
[b]Data from the work of Wu et al. (20).
[c]ATP maintenance rate of 110 mmol ATP h^{-1} gCDW.

enzyme pathways for energy homeostasis, or they fail to predict growth under high-oxygen and high-substrate conditions. By integrating *A. vinelandii*'s energy metabolism dynamics under nitrogen-fixing conditions into the genome-scale metabolic model and constraining the model with high-quality bioreactor data, an accurate growth and partitioning of resources can be predicted. Interestingly, the carbon cost of respiratory protection within the model is not entirely accounted for by decoupling energy through the partially coupled branch. The model also indicates that large amounts of energy are dedicated to maintaining respiratory protection even when fixed nitrogen is in the growth medium under laboratory conditions of high carbon and high oxygen concentrations. Understanding the distribution of flux throughout the ETS is essential in the development of ammonia-excreting diazotrophs. The energy requirements and the metabolic bottlenecks for newly engineered ammonia-excreting strains may be predicted with the model.

The future of agriculture is dependent on an affordable, renewable, and environmentally sound supply of nitrogenous fertilizer. Synthetic biology and BNF have the potential of alleviating some dependency on traditional fertilizing techniques. Nevertheless, an accurate understanding of nitrogen fixation at the systems level is required to maximize high-throughput synthetic biology abilities. The metabolic model presented here is the first step in understanding some of the dynamics of this complex system.

RESULTS

Curation of the metabolic model of *A. vinelandii*. Recently, a metabolic model (iDT1278) was published that encompasses much of the *A. vinelandii* genome, establishing carbon and nitrogen sources using Biolog plate experiments (35). This framework for understanding the metabolism of *A. vinelandii* is a valuable tool for quantifying the production of biopolymers. However, the model iDT1278 lacked essential enzymes required for nitrogen fixation and failed to determine an accurate growth rate in standard laboratory conditions of complete aeration and at least 10 g/L of sucrose or equivalent carbon source (36) (Table 1). Therefore, a new model (iAA1300) presented here expands the iDT1278 model by adding missing reactions and manually curating inadequately annotated constraints (Table S1). Specifically, enzymes of the ETS were added to iAA1300, including Fix, NDHI, a quinone:cytochrome c oxidoreductase, V- and Fe-only nitrogenase, and a transhydrogenase, all of which have been biochemically or genetically determined to play a role during nitrogen fixation.

After manual curation, the model required central carbon metabolism constraints to represent experimental results more accurately. First, unlike other species in the family *Pseudomonadaceae*, *A. vinelandii* contains phosphofructose kinase and has a complete Embden-Meyerhoff pathway (37). Nevertheless, multiple studies have shown that *A. vinelandii* utilizes the Entner-Doudoroff (ED) pathway (20, 38). Flux into the ED pathway and the glyoxylate shunt was constrained to a ratio determined previously by ^{13}C-metabolic

TABLE 2 Experimental measured maintenance and predicted ATP maintenance rate for both branches of the ETS[a]

Carbon source	$[O_2]$ (μM)	Maintenance coefficient ($mmol_{substrate} \cdot h^{-1} \cdot gCDW^{-1}$)[b]	Predicted ATPM ($mmol_{ATP} \cdot h^{-1} \cdot gCDW^{-1}$)	
			Fully coupled	Partially coupled
Sucrose	12	0.9	50.3	16.3
	48	4.4	245.6	78.8
	108	6.2	346.1	110.8
	144	7.0	390.9	125.0
	192	8.0	446.7	143.1
Glucose	108	14.8	364.4	111.4

[a]ATP maintenance rate was determined by setting substrate uptake rate to the maintenance coefficient and increasing ATP maintenance reaction flux until growth rate reached zero.
[b]Maintenance coefficient from the work of Kuhla and Oelze (39), converted from grams of protein to g CDW.

flux analysis (20). While these constraints directed carbon into the correct pathways, the predicted growth rate for model iAA1300 was still inaccurate (Table 1).

Establishing constraints for accurate growth rate determination. Model iAA1300 overestimated growth in almost every condition due to the lack of accurate non-growth-associated maintenance flux (NGAM). Microbiologists since the 1950s have observed that the genus *Azotobacter* has an unusually high respiration rate, leading to increased maintenance requirements (68, 69). The high maintenance and respiration rate of *A. vinelandii* result in low biomass yields compared to other model proteobacteria. Quantitative modeling accurately described this phenomenon with large amounts of energy diverted to respiratory protection (33).

To translate the excess energy consumption into the genome-scale model, experimental data were used to predict an ATP maintenance (ATPM) rate under different O_2 concentrations. Kuhla and Oelze (39) measured maintenance coefficients ($mmol_{substrate} \cdot h^{-1} \cdot g\ CDW^{-1}$; "CDW" is dry weight of cells) of *A. vinelandii* growing in continuous diazotrophic cultures in different O_2 concentrations and carbon sources, using the Pirt method (40) (Table 2). Maintenance coefficients increased as the O_2 concentration increased in the bioreactor. Converting the experimentally determined maintenance coefficient to the genome-scale model ATPM reaction ($mmol_{ATP} \cdot h^{-1} \cdot g\ CDW^{-1}$) requires an ATP/substrate ratio term. An issue arises with converting the maintenance coefficient to ATPM when considering the ATP produced per O_2 consumed (P/O ratio) of the different branches of the ETS. The fully coupled branch uses 1 mol of glucose to produce 32 mol of ATP, but the partially coupled respiratory protection branch produces only 9 mol of ATP per mol of glucose. Experimentally during high substrate and high O_2 conditions, *A. vinelandii* requires decoupling of the ETS through the partially coupled branch to maintain growth (25, 41, 42).

To confirm the use of the partially coupled branch, each path of the ETS network was tested to determine its accuracy to predict the growth rate. Two models were created, the first assuming that all flux to O_2 is directed through NDHI and cytochrome *o* (fully coupled branch) and the second assuming all flux to O_2 through NDHII and cytochrome *bd* (partially coupled branch) (Fig. 1). In both models, substrate uptake rates were set to the experimentally determined maintenance coefficients for each O_2 concentration (39). This uptake rate represents the substrate consumption when no growth occurs; therefore, all energy produced must go to NGAM. To determine the corresponding NGAM for each condition, flux through the reaction ATPM was increased until the growth rate reached zero (Table 2).

The model-determined maintenance rates were then tested to predict growth rates at the different O_2 concentrations. Each model was given an experimental substrate uptake rate and the predicted ATPM flux for each O_2 concentration. Growth rates were then predicted and tested for error against experimental data. Using the fully coupled branch results in growth overestimates for all O_2 concentrations (Fig. 2b). The partially coupled branch model predicted growth rates with a minor error, especially at lower O_2 concentrations (Fig. 2a). The partially coupled model is within reasonable error across all growth rates for O_2 concentrations of 12, 48, and 108 μM (Table S2). Adding

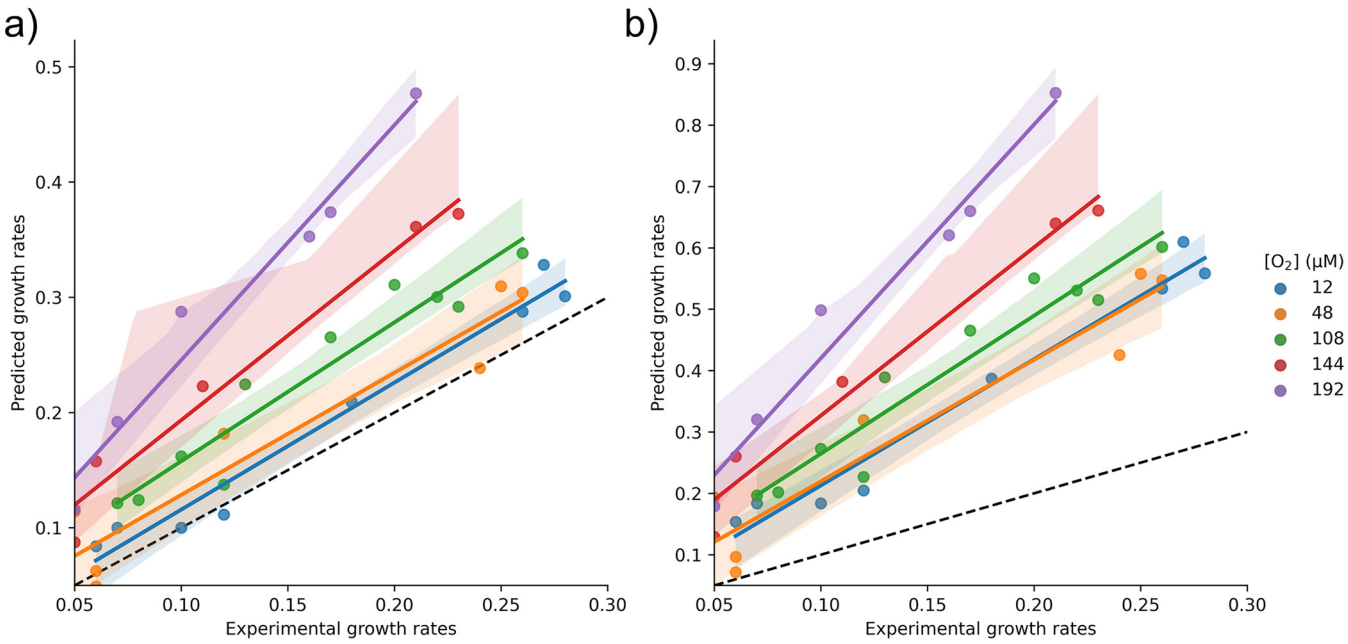

FIG 2 Each model was given an experimentally determined sucrose uptake rate, and a growth rate was predicted. Here, theoretical growth rate and experimental growth rate were compared for diazotrophic growth in different oxygen conditions. Perfect prediction rates follow the $x = y$ dotted line. Shading represents the 95% confidence interval for linear regression fit. (a) Using the partially coupled branch to determine ATPM flux gives an accurate growth rate prediction for lower O_2 concentrations of 12, 48, and 108 μM. Divergence from this trend occurs at 144 and 192 μM O_2, where the model overestimates growth. (b) Using the fully coupled branch of the ETS to determine the ATPM flux causes an overestimation of growth under all conditions.

these maintenance constraints to the model accurately predicts growth (Table 1). For the higher O_2 concentration of 144 and 192 μM, the partially coupled branch model still overestimates growth. For these conditions, the respiratory protection and predicted maintenance could not account for the excess energy expenditure. Therefore, to better predict growth under high O_2 concentration even with the partially coupled branch, more energy allocation to ATPM would limit biomass production, increase respiration, and slow predicted growth.

Assessment of growth yield in response to oxygen concentration. The overall growth efficiencies can be further investigated with detailed maintenance estimates. The growth yield was predicted using the experimental sucrose uptake rate and plotted versus the experimentally determined growth yield (Fig. 3a). Similar to the growth rate predictions, the growth yield predictions indicate that the 12, 48, and 108 μM O_2 conditions are within error. The differentiation of growth yield between the 12 μM condition and higher-O_2 conditions initially seen in the experimental data can be reproduced with the model. The original work of Kuhla and Oelze discussed this effect as the "decoupling of respiration" or respiratory protection (39). However, we have shown that the partially coupled branch is required even at 12 μM O_2. To investigate this phenomenon in more detail, energy allocation during the increase of O_2 concentration was plotted (Fig. 3b). The flux through ATP synthase and O_2 respiration rates (cytochrome *bd*) increase linearly with O_2 concentration. However, partitioning of the ATP differentiates the 12 μM condition from the high O_2 concentrations. The percentage of ATP consumed in ATPM reaction plateaus at around 60% of total ATP consumed for 48, 108, 144, and 192 μM O_2 but only at ~30% for 12 μM O_2. This differentiation allows more ATP to be utilized in biomass production, creating higher growth yields for the 12 μM O_2 concentration.

Ammonia-assimilating conditions require a high maintenance rate for accurate growth. The respiratory protection mechanism was considered to be directly responsible for protecting nitrogenase from O_2 damage (11). Experimentally, growth rates under ammonia-supplemented conditions are similar to those under diazotrophic conditions with high carbon, with comparable biomass yield (15, 20). Modeling

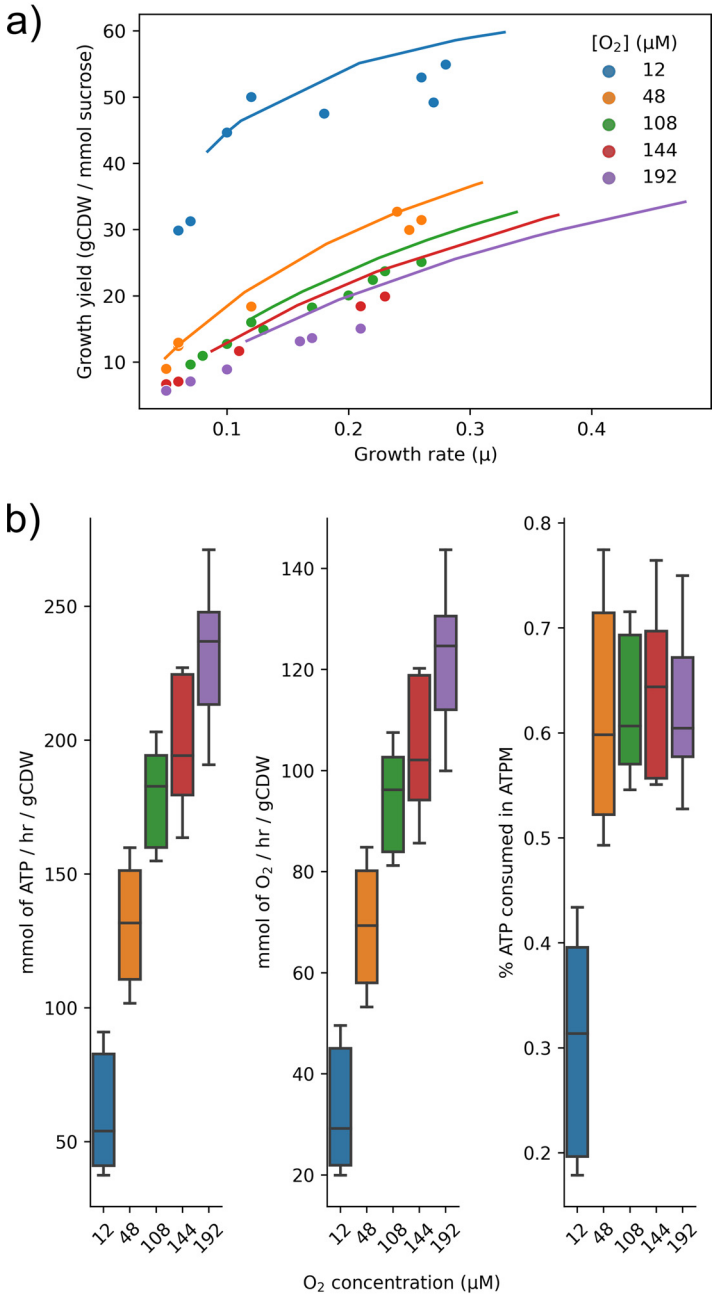

FIG 3 Allocation of carbon and energy at different O_2 concentrations. (a) Predicted growth yields (lines) were plotted for each O_2 concentration across multiple growth rates. Plotted versus experimental growth yields (points) show accurate predictions for lower oxygen concentrations. (b) Resource allocation across multiple O_2 concentrations, sucrose uptake rates, and growth rates. Measured by flux through ATP synthase, respiration rates, and percentage of total ATP consumed in ATPM.

ammonia-supplemented growth shows the requirement of the partially coupled branch to minimize ATPM and accurately predict growth (Table 1). While there is a lack of accurate physiological details on *A. vinelandii* grown in high-carbon and ammonia-supplemented medium, similar respiration rates have been reported (15). The energy allocation under ammonia-supplemented growth shows that the ATP not used in nitrogen fixation is utilized for biomass production (Fig. S1).

Effects of Rnf and Fix on accurate growth predictions. While the model shows the requirement of the partially coupled branch to minimize flux through NGAM, little is known about Rnf and Fix's roles under different O_2 conditions. The use of Rnf or

Fix was considered when the initial ATPM flux was determined, but neither path affected the overall cost of NGAM (Data Set S1). Under high-O_2 conditions, the percent of electron flux required for Fd reduction is minimal compared to that for respiration. However, the different reaction mechanisms suggest that Rnf and Fix might play different roles within the ETS. This difference is accentuated when NDHII is used, as the energy from quinone reduction does not contribute to proton motive force. Therefore, in this scenario, with NDHII as the primary NADH oxidation site, the use of NADH to reduce Fd/Fld using Fix does not sacrifice translocated protons. Fix is favored as the flux increases to nitrogenase and away from O_2 reduction, as it can maintain a higher ATP production rate (Fig. S2). Rnf consumes energy through the proton motive force, lowering growth yields compared to Fix, and increases O_2 consumption, which could help predict high O_2 concentrations more accurately.

Flux sampling analysis reveals the dynamics of the ETS. A flux sampling approach was taken to further understand the network's variability under high- and low-O_2 conditions. While similar in concept to flux variability analysis, flux sampling analysis provides a range of all feasible solutions and allows a distribution of the feasible fluxes, permitting statistics to be used in determining shifts of change between conditions (43). To assess the effect of increased O_2 during nitrogen fixation, the maintenance constraints defined in Table 2 for 108 and 12 μM O_2 were used. To be sure that the constraints produced models dependent only on O_2 concentration, flux balance analysis (FBA) was used to show similar growth rates of 0.202 h^{-1} for 108 and 0.222 h^{-1} for 12 μM O_2. Flux samples were taken and normalized to sucrose uptake rate to compare electron allocation in the model. NADH production in the TCA cycle increased in 108 μM O_2 compared to 12 μM O_2, but flux is decreased in NADH-consuming reactions such as those involving glutamate synthase, relative to carbon uptake (Fig. 4a). The partially coupled branch increases flux under higher O_2 concentrations to protect nitrogenase and supply ATP for the increased maintenance rate. Electron transfer to nitrogenase through Rnf and Fix is reduced in higher O_2 concentrations, while ATP synthase is increased overall, leading to less flux to nitrogenase (Fig. 4b).

Efficient growth under metal-limited conditions. *A. vinelandii* can adapt to the metal availability of its environment by using alternative nitrogenases. While the alternative nitrogenases use more common metals, such as V and Fe, they produce more H_2 and are less efficient at reducing nitrogen than Mo-nitrogenase (equations 2 and 3) (3). This inefficiency of ammonia production acts as an unnecessary sink for electrons, reducing the growth rate of *A. vinelandii* under Mo-limited conditions. Interestingly, while the cost to fix nitrogen rises 30% for V-nitrogenase and 60% for Fe-only nitrogenase, growth rates do not show a complementary decrease (4, 44). This indicates compensation for the larger energy sinks of the alternative nitrogenase.

$$N_2 + 12e^- + 24\mathrm{MgATP} + 12H^+ \rightarrow 2NH_3 + 3H_2 + 24\mathrm{MgADP} + 16P_i \quad (2)$$

$$N_2 + 20e^- + 40\mathrm{MgATP} + 20H^+ \rightarrow 2NH_3 + 7H_2 + 40\mathrm{MgADP} + 16P_i \quad (3)$$

To demonstrate growth under alternative nitrogenase conditions, the 108 μM O_2 model was used, but the flux through Mo-nitrogenase or both Mo- and V-nitrogenase was set to zero for V- and Fe-only conditions, respectively. Growth rates were determined with FBA as well as O_2 uptake rates and flux through each nitrogenase (Table 3). The model shows a slowing of growth by 13% for V conditions and 31% for Fe-only conditions, which follows but is not proportional to the increased cost of nitrogenase turnover. Additionally, only a small increase of flux to O_2 consumption is required to maintain energy production in alternative conditions.

To further investigate the rearrangement of the *A. vinelandii* metabolism to compensate for alternative nitrogenase flux, the flux sampling method was used to determine probabilities for flux changes between conditions. Flux samples were plotted relative to the Mo-nitrogenase flux to determine the alternative nitrogenases' positive or

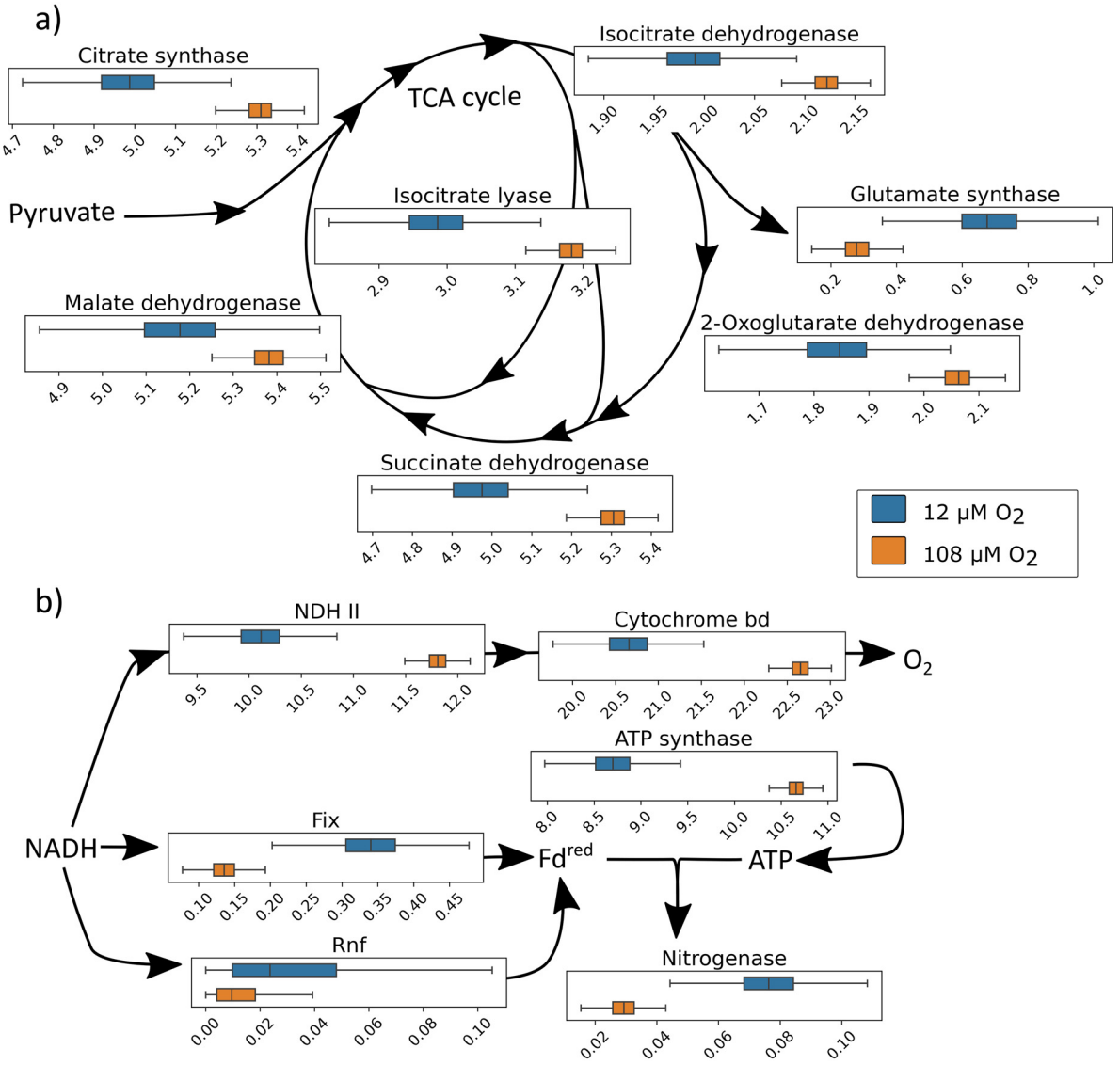

FIG 4 Histogram of flux samples normalized to sucrose uptake at different O_2 concentrations. (a) Key NADH-producing enzymes of the TCA cycle show an increase of flux at higher [O_2] (orange) than lower [O_2] (blue). At the same time, electron-consuming reactions such as glutamate synthase are reduced at high [O_2]. (b) The ETS shifts fluxes to accommodate [O_2], where the partially coupled branch increases flux while electron flux to nitrogenase through ferredoxin (Fd^{red}) is reduced. Flux is driven to oxygen reduction at the expense of nitrogen reduction. ATP generation is still maintained at a high rate to support NGAM in the model.

negative effect (Fig. S3). From the flux sampling, an increase in flux is seen through Fix, as the alternative nitrogenases are less efficient, requiring more reduced Fd. In addition, there is an increase of flux through uptake hydrogenase, which adapts to the increased hydrogen by-product. On the other hand, the flux through NDHII is

TABLE 3 Growth rates and nitrogenase rates decrease while respiration increase as the model switches from Mo- to V- to Fe-only nitrogenase[a]

Nitrogenase	Growth rate (h^{-1})	O_2 consumption ($mmol_{O2} \cdot h^{-1} \cdot g\ CDW^{-1}$)	Nitrogenase flux ($mmol_{N2} \cdot h^{-1} \cdot g\ CDW^{-1}$)
Mo	0.22	98.16	1.04
V	0.17	99.40	0.91
Fe	0.13	101.14	0.72

[a]All data were derived from the model with a sucrose uptake rate of 9 $mmol_{sucrose}$/h/g CDW and an ATP maintenance rate of 110 $mmol_{ATP}$/h/g CDW.

TABLE 4 Table of predicted fluxes for ammonia-assimilating, diazotrophic, and ammonia-excreting (Δ*nifL*) cells grown under high-oxygen (108 μM) and low-oxygen (12 μM) conditions[a]

Conditions	Growth rate (h^{-1})	Value (mmol of metabolite · h^{-1} · g CDW^{-1}) for:			
		Ammonia exchange	Respiration rate	Sucrose uptake	Nitrogenase flux
Ammonia, high O_2	0.30	−3.19	95.24	−9.00	0.00
Ammonia, low O_2	0.33	−3.48	34.07	−4.00	0.00
Diazotrophic, high O_2	0.20	0.00	98.02	−9.00	1.05
Diazotrophic, low O_2	0.22	0.00	37.10	−4.00	1.15
Δ*nifL*, high O_2	0.10	3.00	100.64	−9.00	2.04
Δ*nifL*, low O_2	0.12	3.00	39.71	−4.00	2.14

[a]Negative exchange rates are uptakes into the cell, while positive values are excretions.

decreased, even though overall respiration does not change as electron flux is compensated for by hydrogenase and Fix (Fig. S3).

Optimal ammonia excretion under aerobic nitrogen-fixing conditions. Unlocking *A. vinelandii's* nitrogen fixation regulatory system by deleting the *nifL* gene allows nitrogenase to be constitutively expressed even in the presence of high ammonia concentrations in the medium (36, 45). The ability to engineer a robust ammonia-excreting strain has been a target for genetic engineering for many decades. By simulating the maximum ammonia production by *A. vinelandii*, key insights can be developed for future engineering targets for agricultural or industrial scenarios. To test the viability of ammonia excretion of the model and the effect of O_2 maintenance, models of low and high O_2 (12 and 108 μM O_2) were set to excrete ammonia at a rate of 3 $mmol_{ammonia} \cdot h^{-1} \cdot g\ CDW^{-1}$ as estimated from the work of Plunkett et al. (36). In these simulations, the increase of ammonia excretion essentially doubled the flux through nitrogenase and correspondingly reduced the growth rate (Table 4). Ammonia-excreting strains start to excrete ammonia within the stationary phase during batch growth (36). Cell growth would be minimal under these conditions, and O_2 would be limited due to cell density. As maximal ammonia excretion starts in the early stationary phase, the predicted growth rate might not represent what is happening in the batch culture. Ammonia yields for high and low O_2 are similar to the predicted 1.3 $mol_{sucrose}/mol_{ammonia}$, while ~1.4 $mol_{sucrose}/mol_{ammonia}$ was experimentally determined. When O_2 was increased to reduce the amount of time required for ammonia accumulation, an ammonia yield of ~2.3 $mol_{sucrose}/mol_{ammonia}$ was experimentally determined, and 3 $mol_{sucrose}/mol_{ammonia}$ was predicted (36).

DISCUSSION

The decoupling of energy consumption and biomass accumulation combined with an exceptionally high respiration rate in *A. vinelandii* cells led to the proposal of respiratory protection (46, 47, 68, 69). This proposal was reinforced with the discovery within *A. vinelandii* of a branch of ETS containing the uncoupled NADH dehydrogenase (NDHII) and the terminal oxidase cytochrome *bd* with high V_{max} (maximum reaction velocity) and low affinity for O_2 (11, 22, 25, 41, 48). Others have disagreed with the basic principles of respiratory protection, as nitrogen fixation and O_2 consumption are not correlated (16). The respiration rate plateaus after a concentration of 70 μM O_2 with only a corresponding slight decrease of nitrogenase rate (15). While these observations of plateauing of O_2 respiration are valid, the decoupling of energy from biomass still increases with O_2 concentration. Inomura et al. developed a quantitative mechanistic model showing increased respiratory protection, including maintenance as the O_2 concentration increases (33). The Inomura model relied on an energy transfer efficiency parameter to estimate the efficiency of the ETS to convert carbon into ATP. Using a stoichiometric model, a detailed understanding of flux through each reaction of the ETS can be predicted, allowing one to make an informed hypothesis and to develop engineering strategies.

Using experimental maintenance coefficients and the genome-scale model iAA1300, we have shown that the partially coupled branch of the ETS appears to be involved in metabolism at all measured O_2 concentrations. Requiring the partially coupled branch was based on the need to factor the high *Azotobacter* NGAM into the model, which is very high compared to other genome-scale models of proteobacteria (49, 50). The minimization of NGAM is dependent on the decoupling of the ETS. However, transcript expression and spectrographic data suggest that the fully coupled branch may be active under normal nitrogen-fixing conditions (13, 23, 45, 51). Thus, both branches of the ETS may work together to balance diverse conditions. More significant energy dissipation through the NGAM mechanism would be required to model simultaneous use of both branches.

O_2 reduction and energy production decoupling are not entirely accounted for by the partially coupled branch alone. The extra energy consumption required to maintain accurate growth is modeled as an ATP consumption reaction. This consumption most likely incorporates many different reactions and does not have to be ATP, but two categories can be proposed: (i) base metabolic reactions not accounted for in the model and (ii) reactions that respond to O_2 and dissipate energy. For the first category, more accurate physiological data and biomass composition would help predict energetic needs. The current model predicts growth yields for 12, 44, and 108 μM O_2 concentrations, so a significant change in the biomass equation is not expected (Fig. 4a). The *A. vinelandii* strain OP and derivatives such as strain DJ cannot produce alginate and do not produce poly(3-hydroxybutyrate) under high O_2 and continuous culture (52–55). However, energy-consuming mechanisms like general protein turnover and unknown transport of metabolites or proteins might contribute to the basal NGAM. The second proposed category consists of reactions that respond to the O_2 concentration and could be responsible for the energy dissipation. First, oxygen-dependent protein turnover and reactive O_2 species in high O_2 concentrations are unknown. Characterization of O_2-sensitive *A. vinelandii* mutants showed that only three of 13 had a decreased respiration or catalase rate, leaving mechanisms other than respiratory protection as possibly responsible for O_2 sensitivity (56). Also, cellular processes known to be active during nitrogen fixation are challenging to model in steady state, such as proton leakage, pilus formation, and the *in vivo* stoichiometry of nitrogenase (23, 57, 58). Additionally, other reactions can consume O_2 with a low enough reduction potential, including Mehler reactions or soluble terminal oxidases (59, 60).

Preserving high NGAM through the partially coupled branch is required for growth under ammonia-supplemented conditions. While accurate data with high carbon and high ammonia are lacking, the use of diazotrophic maintenance rates closely predicted growth rates for the ammonia supplement model. Under high sucrose and O_2 concentrations, ammonia-supplemented and nitrogen-fixing *A. vinelandii* strains respire at similar rates and offer similar steady-state protein levels (15), leading to the proposal that respiratory protection is not just a mechanism for nitrogenase protection but a core response to high carbon and O_2 concentrations. The respiratory protection branch is regulated by CydR, an FNR regulatory protein that responds directly to O_2 (25). The terminal oxidase cytochrome *bd* is not required for ammonia-supplemented growth (41). However, cytochrome *d*-deficient mutants grow poorly in ammonia-supplemented medium if not inoculated at high cell density, suggesting a role for cytochrome *d* in the higher-O_2 environment of low-density cultures (41, 51). Using data from the Oelze lab, Inomura et al. proposed control of respiration and nitrogen fixation by the C/N ratio, in which excess substrate respiration increases with the C/N ratio until a point at which the C/N ratio is high enough for nitrogenase to be derepressed (34, 61). Although respiratory protection is more dependent on the C/N ratio than nitrogenase regulation, increased respiration at a high C/N ratio still secondarily protects nitrogenase from oxygen. While under both diazotrophic and ammonia-supplemented conditions, respiration plateaus above ~70 μM O_2 (15), we have shown that an increasing O_2 concentration still requires high NGAM. The decoupling of energy and high NGAM in ammonia-supplemented growth could keep the cytosol in microaerobic or at a low

redox potential to support oxygen-sensitive reactions unrelated to nitrogenase. Alternatively, it may be advantageous under high-carbon conditions to maintain low O_2 to rapidly derepress nitrogenase in variable conditions.

To adapt to higher O_2 concentrations, *A. vinelandii* must increase the availability of electrons. Flux sampling normalized to sucrose uptake shows an increased flux of NADH producing reactions of the TCA cycle and a decreased flux in other reactions, such as those with glutamate synthase, Fix, Rnf, and nitrogenase. As the flux to O_2 reduction and ATP generation increases, the percent of energy allocated to nitrogen-fixing reactions decreases (Fig. S1). This explains why mutations in what should be beneficial enzymes such as Fix or Rnf and uptake hydrogenase do not affect growth under standard high O_2 conditions, as the relative flux to nitrogenase is so small (24, 29, 62). Nevertheless, these reactions become more critical if more energy is allocated to nitrogenase under low-O_2 or Mo-limited conditions. The increasing energy demand is significant under Mo-limited conditions, requiring 30% and 60% more energy for V-nitrogenase and Fe-only nitrogenase, respectively. Interestingly, under batch and continuous culture, *A. vinelandii* grows slightly more slowly in medium lacking Mo or lacking both Mo and V (44). The increased flux through hydrogenase and energy-conserving reactions like that with Fix allows *A. vinelandii* to maintain a higher growth rate. This general pattern shows when Rnf's proton motive force mechanism is compared to Fix's electron bifurcation mechanism. At lower O_2 concentrations, the cell moves away from the energy-decoupling and respiration protection reactions and into maximizing energy production, favoring Fix, which supports the creation of proton motive force and ATP production. While kinetics and thermodynamics also influence the enzymes of the ETS, the stoichiometric pattern shows distinct roles for Rnf and Fix.

BNF can alleviate the cost and damage caused by industrial nitrogenous fertilizer. An ammonia-excreting strain of *A. vinelandii* can support plant growth and is a candidate for biofertilizer (63, 65, 66). Understanding the dynamics of metabolism under ammonia-excreting conditions will be essential to engineering more robust strains. Recent work optimized ammonia-excreting strains and showed 3 $mmol_{ammonia} \cdot h^{-1} \cdot g\ CDW^{-1}$ excreted into the medium (36). Modeling these rates shows a doubling of flux through nitrogenase and a halving of growth rate. Experimentally, ammonia-excreting strains grow at rates similar to that of the wild type (WT), but the accumulation of ammonia in the medium occurs in the stationary phase during batch culture. This suggests that the WT is limited in the log phase by nitrogenase flux and that in the stationary phase, once carbon is low, nitrogenase becomes repressed. In contrast, ammonia-excreting strains are also nitrogenase limited in the exponential phase but cannot regulate nitrogenase in the stationary phase. More dynamic modeling of this phenomenon will allow for more optimization and balance, leading to a technology that will maximize ammonia yield.

Conclusion. We have been able to establish a genome-scale metabolic model of nitrogen fixation and adaptations to O_2. This model gives a blueprint for future engineering strategies in nitrogen fixation and its ability to help offset nitrogenous fertilizer. We have shown that carbon concentration, O_2 concentration, and ammonia supplementation affect the nitrogen fixation model. By adding the ETS to this model, we discovered that the contribution of respiratory protection, which previously was proposed to be a mechanism for diazotrophic conditions, might be a general response to high-carbon and high-O_2 conditions. The cell compensates for allocating resources to an extraordinarily high maintenance rate by lowering growth yields and the rearrangement of the ETS. Future engineering in ammonia-excreting organisms must consider this balance between O_2 reduction and nitrogen fixation and the complex relationship between the two.

MATERIALS AND METHODS

Model curation. To build on the previous model, iDT1278 (35), essential reactions for diazotrophic growth were corrected for stoichiometry and annotation or added to the model (Table S1). See the supplemental methods in Text S1 for further model curation procedures.

Maintenance rate quantification. Maintenance coefficients are taken from Table 1 in the work of Kuhla and Oelze (39) and were converted to $sucrose \cdot h^{-1} \cdot g\ CDW^{-1}$ using a ratio of 0.7 g protein/g CDW (15) and then used as the sucrose uptake rate for the model. Under these conditions, the

assumption is that all energy goes to NGAM, causing a zero growth rate. Therefore, to determine the value of NGAM, the ATPM rate lower bound was increased until the growth reached zero, allowing all sucrose consumption to be allocated to NGAM. The determination of ATPM using this method depends on the ETS efficiency, so the fully coupled branch and the partially coupled branch of the ETS as well as the Rnf or Fix routes were used to determine a separated ATPM (Data Set S1). A specific ATPM flux was determined for each ETS branch under different O_2 concentrations using the experimentally determined maintenance coefficient (Table 2).

Model analysis and availability. See the supplemental methods (Text S1) for further model analysis procedures. All other data are available at https://github.com/alexander-alleman/Azotobactervinelandii_metabolicmodel (doi: 10.5281/zenodo.5184646). Metabolic models are saved in json and smbl format. All analysis and figure creation were documented in Jupyter notebooks.

SUPPLEMENTAL MATERIAL

Supplemental material is available online only.

DATA SET S1, XLSX file, 0.05 MB.

TEXT S1, DOCX file, 0.02 MB.

FIG S1, TIF file, 1.8 MB.

FIG S2, TIF file, 2 MB.

FIG S3, TIF file, 1.6 MB.

TABLE S1, XLSX file, 0.01 MB.

TABLE S2, XLSX file, 0.01 MB.

TABLE S3, XLSX file, 0.01 MB.

ACKNOWLEDGMENTS

We acknowledge Bernd Markus Lange and Michael Kahn for their valuable insight and editorial advice.

This work was supported by the U.S. DOE, Office of Science, Office of Basic Energy Sciences, under award DE-SC0018143 to J.W.P. Partial salary for J.W.P. was supported by the United States Department of Agriculture National Institute of Food and Agriculture, Hatch umbrella project 1015621.

REFERENCES

1. Tittonell P, Giller KE. 2013. When yield gaps are poverty traps: the paradigm of ecological intensification in African smallholder agriculture. Field Crops Res 143:76–90. https://doi.org/10.1016/j.fcr.2012.10.007.
2. Fowler D, Coyle M, Skiba U, Sutton MA, Cape JN, Reis S, Sheppard LJ, Jenkins A, Grizzetti B, Galloway JN, Vitousek P, Leach A, Bouwman AF, Butterbach-Bahl K, Dentener F, Stevenson D, Amann M, Voss M. 2013. The global nitrogen cycle in the twenty-first century. Philos Trans R Soc Lond B Biol Sci 368:1–13. https://doi.org/10.1098/rstb.2013.0164.
3. Mus F, Alleman AB, Pence N, Seefeldt LC, Peters JW. 2018. Exploring the alternatives of biological nitrogen fixation. Metallomics 10:523–538. https://doi.org/10.1039/c8mt00038g.
4. Bishop PE, Jarlenski DM, Hetherington DR. 1982. Expression of an alternative nitrogen fixation system in *Azotobacter vinelandii*. J Bacteriol 150:1244–1251. https://doi.org/10.1128/jb.150.3.1244-1251.1982.
5. Chisnell JR, Premakumar R, Bishop PE. 1988. Purification of a second alternative nitrogenase from a *nifHDK* deletion strain of *Azotobacter vinelandii*. J Bacteriol 170:27–33. https://doi.org/10.1128/jb.170.1.27-33.1988.
6. Darnajoux R, Magain N, Renaudin M, Lutzoni F, Bellenger J-P, Zhang X. 2019. Molybdenum threshold for ecosystem scale alternative vanadium nitrogenase activity in boreal forests. Proc Natl Acad Sci U S A 116:24682–24688. https://doi.org/10.1073/pnas.1913314116.
7. Harris DF, Lukoyanov DA, Shaw S, Compton P, Tokmina-Lukaszewska M, Bothner B, Kelleher N, Dean DR, Hoffman BM, Seefeldt LC. 2018. Mechanism of N_2 reduction catalyzed by Fe-nitrogenase involves reductive elimination of H_2. Biochemistry 57:701–710. https://doi.org/10.1021/acs.biochem.7b01142.
8. Harris DF, Yang Z-Y, Dean DR, Seefeldt LC, Hoffman BM. 2018. Kinetic understanding of N_2 reduction versus H_2 evolution at the E4(4H) Janus state in the three n. Biochemistry 57:5706–5714. https://doi.org/10.1021/acs.biochem.8b00784.
9. Poudel S, Colman DR, Fixen KR, Ledbetter RN, Zheng Y, Pence N, Seefeldt LC, Peters JW, Harwood CS, Boyd ES. 2018. Electron transfer to nitrogenase in different genomic and metabolic backgrounds. J Bacteriol 200:e00757-17. https://doi.org/10.1128/JB.00757-17.
10. Dos Santos PC, Fang Z, Mason SW, Setubal JC, Dixon R. 2012. Distribution of nitrogen fixation and nitrogenase-like sequences amongst microbial genomes. BMC Genomics 13:162. https://doi.org/10.1186/1471-2164-13-162.
11. Poole RK, Hill S. 1997. Respiratory protection of nitrogenase activity in *Azotobacter vinelandii*: roles of the terminal oxidases. FEMS Microbiol Rev 17:303–317. https://doi.org/10.1023/A:1027336712748.
12. Bothe H, Schmitz O, Yates MG, Newton WE. 2010. Nitrogen fixation and hydrogen metabolism in cyanobacteria. Microbiol Mol Biol Rev 74:529–551. https://doi.org/10.1128/MMBR.00033-10.
13. D'Mello R, Hill S, Poole RK. 1994. Determination of the oxygen affinities of terminal oxidases in *Azotobacter vinelandii* using the deoxygenation of oxyleghaemoglobin and oxymyoglobin: cytochrome *bd* is a low-affinity oxidase. Microbiology 140:1395–1402. https://doi.org/10.1099/00221287-140-6-1395.
14. Bertsova YV, Bogachev AV, Skulachev VP. 1997. Generation of protonic potential by the *bd*-type quinol oxidase of *Azotobacter vinelandii*. FEBS Lett 414:369–372. https://doi.org/10.1016/s0014-5793(97)01047-8.
15. Post E, Kleiner D, Oelze J. 1983. Whole cell respiration and nitrogenase activities in *Azotobacter vinelandii* growing in oxygen controlled continuous culture. Arch Microbiol 134:68–72. https://doi.org/10.1007/BF00429410.
16. Oelze J. 2000. Respiratory protection of nitrogenase in Azotobacter species: is a widely held hypothesis unequivocally supported by experimental evidence? FEMS Microbiol Rev 24:321–333. https://doi.org/10.1111/j.1574-6976.2000.tb00545.x.
17. Sabra W, Zeng AP, Lünsdorf H, Deckwer WD. 2000. Effect of oxygen on formation and structure of *Azotobacter vinelandii* alginate and its role in protecting nitrogenase. Appl Environ Microbiol 66:4037–4044. https://doi.org/10.1128/AEM.66.9.4037-4044.2000.
18. Peña C, Peter CP, Büchs J, Galindo E. 2007. Evolution of the specific power consumption and oxygen transfer rate in alginate-producing cultures of

Azotobacter vinelandii conducted in shake flasks. Biochem Eng J 36:73–80. https://doi.org/10.1016/j.bej.2007.02.019.
19. Bertsova YV, Bogachev AV, Skulachev VP. 2001. Noncoupled NADH : ubiquinone oxidoreductase of *Azotobacter vinelandii* is required for diazotrophic growth at high oxygen concentrations. J Bacteriol 183:6869–6874. https://doi.org/10.1128/JB.183.23.6869-6874.2001.
20. Wu C, Herold RA, Knoshaug EP, Wang B, Xiong W, Laurens LML. 2019. Fluxomic analysis reveals central carbon metabolism adaptation for diazotroph *Azotobacter vinelandii* ammonium excretion. Sci Rep 9:13209. https://doi.org/10.1038/s41598-019-49717-6.
21. García A, Ferrer P, Albiol J, Castillo T, Segura D, Peña C. 2018. Metabolic flux analysis and the NAD(P)H/NAD(P)$^+$ ratios in chemostat cultures of *Azotobacter vinelandii*. Microb Cell Fact 17:10–13. https://doi.org/10.1186/s12934-018-0860-8.
22. Bertsova YV, Bogachev AV, Skulachev VP. 1998. Two NADH:ubiquinone oxidoreductases of *Azotobacter vinelandii* and their role in the respiratory protection. Biochim Biophys Acta Bioenerg 1363:125–133. https://doi.org/10.1016/S0005-2728(97)00094-7.
23. Hamilton TL, Ludwig M, Dixon R, Boyd ES, Dos Santos PC, Setubal JC, Bryant DA, Dean DR, Peters JW. 2011. Transcriptional profiling of nitrogen fixation in *Azotobacter vinelandii*. J Bacteriol 193:4477–4486. https://doi.org/10.1128/JB.05099-11.
24. Noar J, Loveless T, Navarro-Herrero JL, Olson JW, Bruno-Bárcena JM. 2015. Aerobic hydrogen production via nitrogenase in *Azotobacter vinelandii* CA6. Appl Environ Microbiol 81:4507–4516. https://doi.org/10.1128/AEM.00679-15.
25. Wu G, Cruz-Ramos H, Hill S, Green J, Sawers G, Poole RK. 2000. Regulation of cytochrome *bd* expression in the obligate aerobe *Azotobacter vinelandii* by *CydR* (Fnr). Sensitivity to oxygen, reactive oxygen species, and nitric oxide. J Biol Chem 275:4679–4686. https://doi.org/10.1074/jbc.275.7.4679.
26. Leung D, Oost J, Kelly M, Saraste M, Hill S, Poole RK. 1994. Mutagenesis of a gene encoding a cytochrome *o*-like terminal oxidase of *Azotobacter vinelandii*: a cytochrome *o* mutant is aero-tolerant during nitrogen fixation. FEMS Microbiol Lett 119:351–357. https://doi.org/10.1111/j.1574-6968.1994.tb06912.x.
27. Lanzilotta WN, Seefeldt LC. 1997. Changes in the midpoint potentials of the nitrogenase metal centers as a result of iron protein—molybdenum-iron protein complex formation. Biochemistry 36:12976–12983. https://doi.org/10.1021/bi9715371.
28. Boyd ES, Garcia Costas AM, Hamilton TL, Mus F, Peters JW. 2015. Evolution of molybdenum nitrogenase during the transition from anaerobic to aerobic metabolism. J Bacteriol 197:1690–1699. https://doi.org/10.1128/JB.02611-14.
29. Ledbetter RN, Garcia Costas AM, Lubner CE, Mulder DW, Tokmina-Lukaszewska M, Artz JH, Patterson A, Magnuson TS, Jay ZJ, Duan HD, Miller J, Plunkett MH, Hoben JP, Barney BM, Carlson RP, Miller AF, Bothner B, King PW, Peters JW, Seefeldt LC. 2017. The electron bifurcating FixABCX protein complex from *Azotobacter vinelandii*: generation of low-potential reducing equivalents for nitrogenase catalysis. Biochemistry 56:4177–4190. https://doi.org/10.1021/acs.biochem.7b00389.
30. Hess V, Schuchmann K, Müller V. 2013. The ferredoxin:NAD$^+$ oxidoreductase (Rnf) from the acetogen *Acetobacterium woodii* requires Na^+ and is reversibly coupled to the membrane potential. J Biol Chem 288:31496–31502. https://doi.org/10.1074/jbc.M113.510255.
31. Curatti L, Brown CS, Ludden PW, Rubio LM, Kustu S. 2005. Genes required for rapid expression of nitrogenase activity in *Azotobacter vinelandii*. Proc Natl Acad Sci U S A 102:6291–6296. https://doi.org/10.1073/pnas.0501216102.
32. Biegel E, Schmidt S, González JM, Müller V. 2011. Biochemistry, evolution and physiological function of the Rnf complex, a novel ion-motive electron transport complex in prokaryotes. Cell Mol Life Sci 68:613–634. https://doi.org/10.1007/s00018-010-0555-8.
33. Inomura K, Bragg J, Follows MJ. 2017. A quantitative analysis of the direct and indirect costs of nitrogen fixation: a model based on *Azotobacter vinelandii*. ISME J 11:166–175. https://doi.org/10.1038/ismej.2016.97.
34. Inomura K, Bragg J, Riemann L, Follows MJ. 2018. A quantitative model of nitrogen fixation in the presence of ammonium. PLoS One 13:e0208282. https://doi.org/10.1371/journal.pone.0208282.
35. Campos DT, Zuñiga C, Passi A, Del Toro J, Tibocha-Bonilla JD, Zepeda A, Betenbaugh MJ, Zengler K. 2020. Modeling of nitrogen fixation and polymer production in the heterotrophic diazotroph *Azotobacter vinelandii* DJ. Metab Eng Commun 11:e00132. https://doi.org/10.1016/j.mec.2020.e00132.
36. Plunkett MH, Knutson CM, Barney BM. 2020. Key factors affecting ammonium production by an *Azotobacter vinelandii* strain deregulated for biological nitrogen fixation. Microb Cell Fact 19:107. https://doi.org/10.1186/s12934-020-01362-9.
37. Chavarría M, Nikel PI, Pérez-Pantoja D, de Lorenzo V. 2013. The Entner-Doudoroff pathway empowers *Pseudomonas putida* KT2440 with a high tolerance to oxidative stress. Environ Microbiol 15:1772–1785. https://doi.org/10.1111/1462-2920.12069.
38. Wong TY, Yao X-T. 1994. The DeLey-Doudoroff pathway of galactose metabolism in *Azotobacter vinelandii*. Appl Environ Microbiol 60:2065–2068. https://doi.org/10.1128/aem.60.6.2065-2068.1994.
39. Kuhla J, Oelze J. 1988. Dependency of growth yield, maintenance and Ks-values on the dissolved oxygen concentration in continuous cultures of *Azotobacter vinelandii*. Arch Microbiol 149:509–514. https://doi.org/10.1007/BF00446753.
40. Pirt SJ. 1965. The maintenance energy of bacteria in growing cultures. Proc R Soc Lond B Biol Sci 163:224–231. https://doi.org/10.1098/rspb.1965.0069.
41. Kelly MJ, Poole RK, Yates MG, Kennedy C. 1990. Cloning and mutagenesis of genes encoding the cytochrome *bd* terminal oxidase complex in *Azotobacter vinelandii*: mutants deficient in the cytochrome *d* complex are unable to fix nitrogen in air. J Bacteriol 172:6010–6019. https://doi.org/10.1128/jb.172.10.6010-6019.1990.
42. Kolonay JF, Maier RJ. 1997. Formation of pH and potential gradients by the reconstituted *Azotobacter vinelandii* cytochrome *bd* respiratory protection oxidase. J Bacteriol 179:3813–3817. https://doi.org/10.1128/jb.179.11.3813-3817.1997.
43. Herrmann HA, Dyson BC, Vass L, Johnson GN, Schwartz J-M. 2019. Flux sampling is a powerful tool to study metabolism under changing environmental conditions. NPJ Syst Biol Appl 5:32. https://doi.org/10.1038/s41540-019-0109-0.
44. Natzke J, Noar JD, Bruno-Bárcena JM. 2018. *Azotobacter vinelandii* nitrogenase activity, hydrogen production, and response to oxygen exposure. Appl Environ Microbiol 84:e01208-18. https://doi.org/10.1128/AEM.01208-18.
45. Barney BM, Plunkett MH, Natarajan V, Mus F, Knutson CM, Peters JW. 2017. Transcriptional analysis of an ammonium excreting strain of *Azotobacter vinelandii* deregulated for nitrogen fixation. Appl Environ Microbiol 83:e01534-17. https://doi.org/10.1128/AEM.01534-17.
46. Dalton H, Postgate JR. 1968. Effect of oxygen on growth of *Azotobacter chroococcum* in batch and continuous cultures. Microbiology 54:463–473.
47. Phillips DH, Johnson MJ. 1961. Measurement of dissolved oxygen in fermentations. Biotechnol Bioeng 3:261–275. https://doi.org/10.1002/jbmte.390030306.
48. Ackrell BAC, Jones CW. 1971. The respiratory system of *Azotobacter vinelandii*. Eur J Biochem 20:22–28. https://doi.org/10.1111/j.1432-1033.1971.tb01357.x.
49. Nogales J, Mueller J, Gudmundsson S, Canalejo FJ, Duque E, Monk J, Feist AM, Ramos JL, Niu W, Palsson BO. 2020. High-quality genome-scale metabolic modelling of *Pseudomonas putida* highlights its broad metabolic capabilities. Environ Microbiol 22:255–269. https://doi.org/10.1111/1462-2920.14843.
50. Feist AM, Zielinski DC, Orth JD, Schellenberger J, Herrgard MJ, Palsson BØ. 2010. Model-driven evaluation of the production potential for growth-coupled products of *Escherichia coli*. Metab Eng 12:173–186. https://doi.org/10.1016/j.ymben.2009.10.003.
51. D'mello R, Purchase D, Poole RK, Hill S. 1997. Expression and content of terminal oxidases in *Azotobacter vinelandii* grown with excess NH_4^+ are modulated by O_2 supply. Microbiology (Reading) 143:231–237. https://doi.org/10.1099/00221287-143-1-231.
52. Castillo T, Heinzle E, Peifer S, Schneider K, Pena C. 2013. Oxygen supply strongly influences metabolic fluxes, the production of poly(3-hydroxybutyrate) and alginate, and the degree of acetylation of alginate in *Azotobacter vinelandii*. Process Biochem 48:995–1003. https://doi.org/10.1016/j.procbio.2013.04.014.
53. Díaz-Barrera A, Urtuvia V, Padilla-Córdova C, Peña C. 2019. Poly(3-hydroxybutyrate) accumulation by *Azotobacter vinelandii* under different oxygen transfer strategies. J Ind Microbiol Biotechnol 46:13–19. https://doi.org/10.1007/s10295-018-2090-9.
54. Martínez-Salazar JM, Moreno S, Nájera R, Boucher JC, Espín G, Soberón-Chávez G, Deretic V. 1996. Characterization of the genes coding for the putative sigma factor AlgU and its regulators MucA, MucB, MucC, and MucD in *Azotobacter vinelandii* and evaluation of their roles in alginate

biosynthesis. J Bacteriol 178:1800–1808. https://doi.org/10.1128/jb.178.7.1800-1808.1996.
55. Setubal JC, dos Santos P, Goldman BS, Ertesvåg H, Espin G, Rubio LM, Valla S, Almeida NF, Balasubramanian D, Cromes L, Curatti L, Du Z, Godsy E, Goodner B, Hellner-Burris K, Hernandez JA, Houmiel K, Imperial J, Kennedy C, Larson TJ, Latreille P, Ligon LS, Lu J, Maerk M, Miller NM, Norton S, O'Carroll IP, Paulsen I, Raulfs EC, Roemer R, Rosser J, Segura D, Slater S, Stricklin SL, Studholme DJ, Sun J, Viana CJ, Wallin E, Wang B, Wheeler C, Zhu H, Dean DR, Dixon R, Wood D. 2009. Genome sequence of *Azotobacter vinelandii*, an obligate aerobe specialized to support diverse anaerobic metabolic processes. J Bacteriol 191:4534–4545. https://doi.org/10.1128/JB.00504-09.
56. Iwahashi H, Hachiya Y, Someya J. 1991. Isolation and characterization of oxygen sensitive mutants of *Azotobacter vinelandii*. FEMS Microbiol Lett 77:73–78. https://doi.org/10.1111/j.1574-6968.1991.tb04324.x.
57. Haaker H, Klugkist J. 1987. The bioenergetics of electron transport to nitrogenase. FEMS Microbiol Lett 46:57–71. https://doi.org/10.1111/j.1574-6968.1987.tb02452.x.
58. Hoffman BM, Lukoyanov D, Yang ZY, Dean DR, Seefeldt LC. 2014. Mechanism of nitrogen fixation by nitrogenase: the next stage. Chem Rev 114:4041–4062. https://doi.org/10.1021/cr400641x.
59. Varghese F, Kabasakal BV, Cotton CAR, Schumacher J, Rutherford AW, Fantuzzi A, Murray JW. 2019. A low-potential terminal oxidase associated with the iron-only nitrogenase from the nitrogen-fixing bacterium *Azotobacter vinelandii*. J Biol Chem 294:9367–9376. https://doi.org/10.1074/jbc.RA118.007285.
60. Sarkar D, Landa M, Bandyopadhyay A, Pakrasi HB, Zehr JP, Maranas CD. 2021. Elucidation of trophic interactions in an unusual single-cell nitrogen-fixing symbiosis using metabolic modeling. PLoS Comput Biol 17:e1008983. https://doi.org/10.1371/journal.pcbi.1008983.
61. Bühler T, Sann R, Monter U, Dingler C, Kuhla J, Oelze J. 1987. Control of dinitrogen fixation in ammonium-assimilating cultures of Azotobacter vinelandii. Arch Microbiol 148:247–251. https://doi.org/10.1007/BF00414820.
62. Linkerhägner K, Oelze J. 1995. Hydrogenase does not confer significant benefits to *Azotobacter vinelandii* growing diazotrophically under conditions of glucose limitation. J Bacteriol 177:6018–6020. https://doi.org/10.1128/jb.177.20.6018-6020.1995.
63. Ambrosio R, Ortiz-Marquez JCF, Curatti L. 2017. Metabolic engineering of a diazotrophic bacterium improves ammonium release and biofertilization of plants and microalgae. Metab Eng 40:59–68. https://doi.org/10.1016/j.ymben.2017.01.002.
64. Reference deleted.
65. Mus F, Crook MB, Garcia K, Garcia Costas A, Geddes BA, Kouri E-DD, Paramasivan P, Ryu M-H, Oldroyd GED, Poole PS, Udvardi MK, Voigt CA, Ané J-M, Peters JW. 2016. Symbiotic nitrogen fixation and challenges to extending it to non-legumes. Appl Environ Microbiol 82:3698–3710. https://doi.org/10.1128/AEM.01055-16.
66. Aasfar A, Bargaz A, Yaakoubi K, Hilali A, Bennis I, Zeroual Y, Meftah Kadmiri I. 2021. Nitrogen fixing Azotobacter species as potential soil biological enhancers for crop nutrition and yield stability. Front Microbiol 12:354. https://doi.org/10.3389/fmicb.2021.628379.
67. Lozano E, Galindo E, Peña CF. 2011. Oxygen transfer rate during the production of alginate by *Azotobacter vinelandii* under oxygen-limited and non-oxygen-limited conditions. Microb Cell Fact 10:13. https://doi.org/10.1186/1475-2859-10-13.
68. Parker CA. 1954. Effect of oxygen on the fixation of nitrogen by Azotobacter. Nature 173:780–781. https://doi.org/10.1038/173780b0.
69. Parker CA, Scutt PB. 1960. The effect of oxygen on nitrogen fixation by Azotobacter. Biochim Biophys Acta 38:230–238. https://doi.org/10.1016/0006-3002(60)91236-1.